



<http://www.diva-portal.org>

## Postprint

This is the accepted version of a paper published in *Thin Solid Films*. This paper has been peer-reviewed but does not include the final publisher proof-corrections or journal pagination.

Citation for the original published paper (version of record):

Ericson, T., Kubart, T., Scragg, J., Platzer-Björkman, C. (2012)  
Reactive sputtering of precursors for Cu<sub>2</sub>ZnSnS<sub>4</sub> thin film solar cells.  
*Thin Solid Films*, 520(24): 7093-7099  
<http://dx.doi.org/10.1016/j.tsf.2012.08.002>

Access to the published version may require subscription.

N.B. When citing this work, cite the original published paper.

Permanent link to this version:

<http://urn.kb.se/resolve?urn=urn:nbn:se:uu:diva-183573>

# Reactive sputtering of precursors for $\text{Cu}_2\text{ZnSnS}_4$ thin film solar cells

Tove Ericson\*, Tomas Kubart, Jonathan J. Scragg, Charlotte Platzer-Björkman

Ångström Solar Center, Solid State Electronics, Uppsala University, Box 534, SE-75121

Uppsala, Sweden

\*Corr. author: tove.ericson@angstrom.uu.se, phone: +46-18-4717255, fax: +46-18-555095

## Abstract

The quaternary semiconductor  $\text{Cu}_2\text{ZnSnS}_4$  (CZTS) is a possible In-free replacement for  $\text{Cu}(\text{In,Ga})\text{Se}_2$ . Here we present reactive sputtering with the possibility to obtain homogeneous CZTS-precursors with tunable composition and a stoichiometric quantity of sulfur. The precursors can be rapidly annealed to create large grained films to be used in solar cells. The reactive sputtering process is flexible, and morphology, stress and metal and sulfur contents were varied by changing the  $\text{H}_2\text{S}/\text{Ar}$ -flow ratio, pressure and substrate temperature. A process curve for the reactive sputtering of CZTS from CuSn and Zn targets is presented. The Zn-target is shown to switch to compound mode earlier and faster compared to the CuSn-target. The precursors containing a stoichiometric amount of sulfur exhibit columnar grains, have a crystal structure best matching ZnS and give a broad peak, best matching CZTS, in Raman scattering. Comparing process gas flows it is shown that the sulfur content is strongly dependent on the  $\text{H}_2\text{S}$  partial pressure but the total pressures compared in this study have little effect on the precursor properties. Increasing the substrate temperature changes the film composition due to the high vapour pressures of Zn, SnS and S. High substrate temperatures also give slightly denser and increasingly oriented films. The precursors are under compressive stress, which is reduced with higher deposition temperatures.

**Keywords:**  $\text{Cu}_2\text{ZnSnS}_4$ , CZTS, kesterite, reactive sputtering, process curve, photovoltaics

## 1. Introduction

In recent years the quaternary semiconductor  $\text{Cu}_2\text{ZnSn}(\text{S, Se})_4$  (CZTSSe) has attracted interest as a possible In-free replacement for  $\text{Cu}(\text{In,Ga})\text{Se}_2$  (CIGS). Research is on-going and the current world record efficiency is just over 10 % [1]. There is also work done on the pure selenide (CZTSe) and the pure sulfide (CZTS), which have so far reached record efficiencies of 9.15% [2] and 8.4 % [3] respectively. Several production methods have been investigated, both vacuum and non-vacuum, for example sputtering [4], evaporation [5], electrodeposition [6] and solution based techniques[1]. Most successful so far are the two step methods containing a deposition step, which gives an homogeneous film with full chalcogen content, and then a short annealing step to allow the film to crystallize into CZTSSe [1]. It is suggested that this is because the CZTSSe risks decomposing at high temperatures and/or low pressures

[7], meaning that it is not well-suited to single-step vacuum deposition at high temperature, which is the typical approach for CIGS.

An attractive way of obtaining a precursor for CZTS with these characteristics, a homogeneous film of tunable composition, is to reactively co-sputter Cu, Zn and Sn in H<sub>2</sub>S atmosphere. A rapid anneal can then be used to transform the precursor into a large grained film suitable for solar cells, we have by this approach so far achieved solar cell efficiencies up to 4.6% for CZTS [8].

This work focuses on the preparation and characterization of the precursors produced in the first step. The influence of the annealing process on device performance will be reported in future publications.

The reactive sputtering process is flexible and several parameters, such as pressure, power, substrate temperature and H<sub>2</sub>S/Ar-ratio can be adjusted to vary the crystallinity, density, stress, sulfur content and metal composition of the films. Another advantage of magnetron sputtering is the possibility of easy up-scaling which is important for large scale production.

Previously only a few publications describe reactively sputtered CZTS. In 2010 Liu et al. studied the properties of their dense reactively sputtered CZTS films [9] and the same year Chawla et al. produced reactively sputtered CZTS solar cells in a one step process and achieved an efficiency of 1.35 % [10]. Grain boundary properties of 3.37 % efficiency reactively sputtered and annealed CZTS were investigated in [11]. The present paper focuses on describing the reactive sputtering process in detail and linking variations in the process parameters to film characteristics. This enables us to tailor precursors that are optimal for solar cell fabrication.

Reactive sputtering is most common for oxides and nitrides but has also been investigated for several sulfides and selenides. Especially interesting for the reactive sputtering of CZTS is the work done on other solar cell materials such as CuInS<sub>2</sub> (CIS) and CuInSe<sub>2</sub> (CISE). In the 1980s Thornton et al. carefully investigated the process for reactively sputtered CISE [12, 13]. Reactively sputtered CIS precursors, which were thereafter sulfurized, were investigated by Watanabe et al. in the mid-90s and efficiencies of 6.3 % were reported [14]. In the beginning of the new millennium, He et al. reported on one stage reactively sputtered CIS [15, 16] and in 2008 Seeger and Ellmer presented CIS solar cells with efficiencies of 11.4 % fabricated by one step reactive sputtering [17]. They also concluded that the intrinsic electronic properties of the absorbers produced by this method were excellent. The reason for varying efficiencies was microscopic defects giving shunting problems between front and back contact. A common drawback of one stage sputtering processes is otherwise the presence of energetic negative ions originating from the target surface. These ions have energies up to the full target potential and can create atomic-scale defects in the growing film that degrade the solar cell performance. However, in a two stage process many of these defects can be annealed out in the second step.

## 2. Material and methods

Film depositions were performed in a Von Ardenne CS600 sputtering system with two magnetrons and a front side heater, all facing the substrate with an angle of 45° at 160 mm distance. The targets were 102 mm in diameter and 6 mm thick. Due to the limited number of magnetrons, a CuSn-alloy-target together with a Zn-target (purity 99.994-99.995 %) were

used. Choosing an alloy target also overcomes the issues of the low melting point of Sn. Two different CuSn-alloys were used, one with composition Cu: 67 at % and Sn: 33 at% (purity 99.99 %) and one with Cu: 65 at% and Sn: 35 at% (purity 99.999 %). Pulsed DC with a frequency of 20 kHz was supplied by two Huttinger PFG 3000 DC power supplies equipped with Advanced Energy Sparc-le 20 pulsing units. Both targets were operated in constant power mode with the power ranges 520-600 W for the CuSn-target and 330-480 W for the Zn-target. The base pressure was below  $10^{-4}$  Pa. H<sub>2</sub>S with purity of 99.5% was supplied solely or together with Ar at mass flow rates between 0 and 30 sccm giving a constant total pressure of 0.67 or 1.33 Pa. The maximum setting for the radiative front side heater was 500°C, yielding a maximum temperature at the substrate of approximately 300 °C. The sputtering time was typically 10-30 min.

Three different substrates were used for depositions: glass for profilometer thickness measurements, silicon wafer for sulfur content measurement and Mo-coated glass for other characterization techniques and solar cell fabrication. For the temperature series, an additional 100 μm thick, Mo-coated glass piece (cover glass D 263<sup>®</sup> M from Schott) was included to measure stress in the films. The curvature along two perpendicular directions was measured with a Veeco Dektak 150 profilometer before and after precursor deposition. Since the substrate had a curvature from the Mo-deposition, which was not equal in the two directions, the measurement direction was marked and the comparison was made to the post-deposition measurement from the same direction. The curvatures were fitted by a least squares method. The resulting radii were used to calculate the stress,  $\sigma$ , with the equation  $\sigma = (1/6)((1/r_{post}) - (1/r_{pre}))(E/(1-\nu))(t_s^2/t_f)$  [18] where  $r_{pre}$  and  $r_{post}$  are the radii before and after the precursor deposition,  $E$  is the Young modulus for the glass (72.9 kN/mm<sup>2</sup>, given by the manufacturer),  $\nu$  is the Poisson ratio for the glass (0.208, given by the manufacturer) and  $t_s$  and  $t_f$  are the thickness of the substrate and film respectively.

The metal composition of the films was determined by x-ray fluorescence (XRF) in a PANalytical Epsilon 5. The XRF counts were correlated to metal composition via a thickness series measured by Rutherford backscattering (RBS). The RBS measurements were done at Uppsala Tandem Laboratory (Ion Technology Center) with a 2 MeV He<sup>+</sup>- beam and a backscattering angle of 170 degrees. Since Cu and Zn overlap in RBS, one series with Zn and one with CuSn was used to determine the metal content in a calibration piece. This piece was then measured together with the unknown samples in XRF. The values were corrected for attenuation of out-going characteristic x-rays. The sulfur content of the films was measured with energy dispersive spectroscopy (EDS) at 20 keV, in a LEO 440 SEM with an EDAX EDS system. These measurements were made on samples on Si-wafer substrates instead of Mo-coated glass, because S and Mo signals overlap in EDS.

Thickness measurements were made with a Veeco Dektak 150 profilometer and by scanning electron microscopy (SEM) of cross sections using a LEO 1550. A Siemens D5000 was used for grazing incidence x-ray diffraction (GI-XRD) at 1° incidence angle in parallel beam geometry and for  $\theta$ -2 $\theta$  XRD in Bragg-Brentano focusing geometry. For both techniques CuK $\alpha$  radiation was used. The XRD peak shift in the temperature series was determined by stripping the signal from K $\alpha_2$  and fitting the peak with PANalytical High Score Plus. Raman scattering was measured with a Reinshaw system at an excitation wavelength of 514 nm.

### 3. Results and discussion

Two distinct modes of operation exist in reactive magnetron sputtering depending on the state of the sputtering target [19]. Starting with operation in pure Ar, the target surface is metallic. With increasing mass flow of the reactive gas, a compound starts to form at the target surface, and when the surface is fully covered by this layer the target is referred to as being in compound mode. Depending on the material system, the difference in sputtering yield between metal and compound, and the configuration of the sputtering system, the transition between these two modes can be abrupt or gradual. In the case of an abrupt transition, a hysteresis effect is often seen. The change in the surface composition has a pronounced effect on the ion-induced secondary electron yield, which in turn is the main determinant of the discharge voltage. Observing the discharge voltage can therefore serve as a measure of the surface status of the target [20]. Formation of a compound at the surface is also accompanied by a change in the sputtering yield and hence the deposition rate, which can also be used as a measure of the transition between modes. In order to characterize a sputtering process, a process curve is typically used. It shows the process parameters as a function of the reactive gas flow.

The process curve for this system is shown in Figure 1. Increasing the H<sub>2</sub>S flow from 0 sccm to 5 sccm does not significantly influence the voltage on the CuSn-target. However, the voltage on the Zn-target drops significantly indicating that the majority of the supplied H<sub>2</sub>S is consumed by the Zn and this target is sulfurized first. This agrees with ZnS having a more negative free energy of formation than Cu-S and Sn-S compounds. The abrupt transition indicates high reactivity and large difference in sputtering yield between Zn and ZnS. The voltage decrease indicates an increase in secondary electron yield for ZnS and this agrees well with earlier reports [21]. Increasing the H<sub>2</sub>S flow further leads to formation of a compound also on the CuSn-target. This transition from metal to compound mode is more gradual and the voltage continuously increases from around 500 V at 5 sccm to 580 V at the end point of 20 sccm H<sub>2</sub>S. This agrees with earlier work which reported an increase in voltage for reactive sputtering of pure Cu in H<sub>2</sub>S [22]. For Cu it has also been shown that it has long time constants for equilibration, where the final stable voltage in constant H<sub>2</sub>S flow rate was not seen until after sputtering for about 30 min [23]. This is an indication that a CuSn-target could need a long sputtering time before it reaches a fully stable state in compound mode and this should be accounted for in order to achieve a stable process. As can be seen in Figure 1, no hysteresis was observed for the sputtering process.

In order to further characterize the deposition process, four samples were deposited (Series 1: sample A, B, C and D, Table I). The H<sub>2</sub>S/Ar-flow ratio was changed while the other process parameters were kept constant with 600 W on the CuSn-target, 330 W on the Zn-target, 800 s sputtering time and a 0.67 Pa process pressure. As expected, the transition from metal to compound mode can be seen when comparing the amount of deposited metal for each sample, on the right axis in Figure 1. The Zn-rate drops quickly as a result of lower sputtering yield of ZnS while the CuSn-rate decrease slowly, agreeing well with the metal-to-compound transition types observed with the voltage measurement. Due to the difference in transition behavior the deposited samples vary in Zn-content, as can be seen in Table I. The purely metallic sample, A, is very Zn-rich, since the deposition rate from the metallic Zn target is high. When H<sub>2</sub>S is added, the Zn-rate drops rapidly and samples B and C are Zn-poor. At the highest H<sub>2</sub>S flow rate used, sample D, the CuSn-rate has decreased enough to result in a higher relative Zn-content. The sulfur content of the film increases fairly linearly with increasing H<sub>2</sub>S flow, and the films sputtered in pure H<sub>2</sub>S have, according to EDS, a close to stoichiometric sulfur content of 51 at%.

Figure 2 shows the GIXRD for the samples in Series 1. Sample A, sputtered without H<sub>2</sub>S, shows reflections from elemental Sn [24] and Cu<sub>5</sub>Zn<sub>8</sub> [25]. Comparing this with the phase diagram in [26] (shown for 180-250°C) we would have expected Sn, CuZn and Cu<sub>6</sub>Sn<sub>5</sub> for this composition. However, we are fairly close to the region in the phase diagram in which Sn and Cu<sub>5</sub>Zn<sub>8</sub> are expected, so considering the non-equilibrium conditions present during sputtering this is not an unreasonable result. Also stated in [26] is that the reason for forming a CuZn-compound is the high reactivity of Zn and that Cu diffuses easily. For sample B, where the process gas is 50 % H<sub>2</sub>S, the film sputtered is mostly amorphous with only two very broad peaks seen at around 28.6° and 42.5°. The first one matches the most intense peaks from sphalerite ZnS [27] and the second one fits well with the most intense peak of several CuSn-phases, for example Cu<sub>40</sub>Sn<sub>11</sub> [28]. This also agrees with the process curve (Figure 1) which indicates that the Zn-target should be sulfurized at this point but the CuSn-target is in the transition between metal and compound mode. The two samples sputtered at higher H<sub>2</sub>S-flow both show reflections from a zinc blende structure. These peaks are common for CZTS [29], Cu<sub>2</sub>SnS<sub>3</sub>[30-32] (CTS) and sphalerite ZnS with small shifts. None of the weak reflections specific for CZTS or CTS were observed. We will hereafter refer to this pattern as  $\Sigma$ , following the notation introduced in [33]. The  $\Sigma$  peaks are more intense for the fully sulfurized sample and here also an unidentified shoulder just below the main peak is seen. In all samples the two strongest reflections from the back contact Mo [34] can be observed.

From Raman scattering (Figure 3), no clear peaks can be seen for the metallic (A) and the low sulfur film (B). For samples C and D a clear but broad peak at 336 and 332 cm<sup>-1</sup> respectively is seen. Peak fitting with Lorentzian curves for sample D gave good agreement for four peaks between 200 and 500 cm<sup>-1</sup>. The resulting peak positions for the weaker contributions are at 256 cm<sup>-1</sup>, 290 cm<sup>-1</sup> and 354 cm<sup>-1</sup>. According to Himmrich et al., [35], Raman scattering from CZTS should show three peaks at 285, 336 and 362 cm<sup>-1</sup> where the middle peak is most intense. They also report several IR peaks and the peak at 255 cm<sup>-1</sup> agrees well with our peak fitted at 256 cm<sup>-1</sup>. The other peak positions suggested from the fit are close to the three Raman frequencies reported and have similar intensity distribution. CZTS is therefore a plausible match for the sample. However, as described in [36] several other compounds have intensities in the same range, such as ZnS, Cu<sub>2</sub>SnS<sub>3</sub> and Cu<sub>3</sub>SnS<sub>4</sub>, and cannot be ruled out.

The SEM-images (Figure 4) confirms the crystallinity information from the XRD measurement. Sample B appears mostly amorphous and samples A, C and D crystalline. However, samples C and D have a clear columnar structure while sample A appears more disordered. This is possibly due to the structural difference between Sn and Cu<sub>5</sub>Zn<sub>8</sub> compared to the similarities between CZTS, ZnS and CTS, or due to the lower melting point of Cu<sub>5</sub>Zn<sub>8</sub> and Sn compared to the sulfides.

To study the influence of process pressure a series with two different pressures, 0.67 and 1.33 Pa, and three different H<sub>2</sub>S/Ar-ratios, was deposited (Series 2: samples E-5, E-10, F-5, F-10, G-5 and G-10, see Table II). The other process parameters were kept constant with 600 W on the CuSn-target, 330 W on the Zn-target and a deposition time of 800 s. The total gas flow was 30 sccm. The process curve taken at 1.33 Pa (not shown) is similar to the one presented in Figure 1 but also shows that the CuSn-target voltage levels out at about H<sub>2</sub>S/Ar: 25/5 sccm. However, already at 20/10 sccm (sample F-10) the film is almost fully sulfurized with a sulfur content of 49 at% (Table II). This sample shows a clear but quite broad peak at 330 cm<sup>-1</sup> in Raman and the  $\Sigma$ - reflections in XRD, similar to the Raman response and diffractogram from sample D in series 1 and therefore not shown. The XRD peaks are more pronounced for the sample sputtered in pure H<sub>2</sub>S, G-10, but the Raman measurement looks similar. According to EDS measurement the sample sputtered in 30 sccm H<sub>2</sub>S flow contains 54 at% sulfur. This is

within the margin of error from 50at%, which would be stoichiometric CZTS, but it could indicate that the EDS is slightly overestimating the sulfur content. Reasons for a high sulfur content could otherwise be CuS and SnS<sub>2</sub> secondary phases in the film or incorporation of elemental sulfur, but no indication of these are observed with XRD or Raman.

Sample E-10, at H<sub>2</sub>S/Ar: 10/20 sccm, contains 26 at% sulfur according to the EDS and is mainly amorphous, both judging from the SEM images and the XRD pattern (not shown). The XRD of this sample is very similar to that of sample B in series 1, probably because the partial pressure of H<sub>2</sub>S is similar for both deposition processes. When decreasing the process pressure to 0.67 Pa, sample E-5, an additional peak at 36.3° appears in the XRD pattern (not shown). The peak matches the close packed plane for elemental Zn [37] and could indicate that this setting does not supply high enough partial pressure of sulfur to completely react the Zn at the substrate. Besides this difference, the films made at 0.67 and 1.33 Pa are very similar.

The substrate temperature during deposition is predicted to affect the morphology and stress in the film due to increased surface mobility of the arriving atoms [38, 39]. To investigate this, a temperature series was made (Series 3). The second CuSn-target, with composition Cu: 65 at % and Sn: 35 at%, was used for this series. All process parameters besides the substrate temperature were kept constant (Table III). The substrate temperature was varied between room temperature and about 300 °C and, as can be seen in Table III, several parameters were affected. The composition changed both in Cu/Sn-ratio, Zn-content and sulfur content. Comparing the raw XRF signals from the metals (not shown) the difference is mainly due to a decrease of Zn and Sn with increasing temperature. This is probably due to the high vapour pressure of Zn and SnS. The lower sulfur content at higher temperatures can be assigned to the high vapour pressure of S<sub>2</sub>. This agrees with similar processes for CIS where it was observed that, at higher substrate temperatures, a higher H<sub>2</sub>S-flow was needed to achieve the same sulfur content in the films [15].

The decreasing deposition rates would naturally yield thinner films if the density is constant. This is also the case for this series and can be seen in Table III. However, using the metals' areal density from the XRF measurement together with the sulfur content from EDS and the thickness, the density was calculated and it was observed that the decrease cannot only be attributed to fewer atoms in the film but that the high temperature films are also truly denser (Table III). This also agrees with sputtering theory where films deposited at low temperatures are generally less dense.

SEM images of the room temperature deposition and the highest temperature deposition are shown in Figure 5. Comparing these with a general structure zone model (SZM) for sputtering [38], the low temperature depositions exhibit features of zone 1-zone T with a columnar structure and rounded surface. The high temperature deposition appearance is closer to zone T-zone 2 morphology due to the faceted surface and angled grain boundaries within the film. When calculating the approximate T/T<sub>m</sub> for these depositions it agrees well with what is expected from the SZM.

The Raman measurements for the samples in series 3 (not shown) are similar to sample D from series 1 and show a peak at 334 cm<sup>-1</sup>. XRD (Figure 6) shows the  $\Sigma$ -pattern and the unidentified shoulder just below the main peak at 28° for all the depositions. The intensities of the peaks changes within the series. The main peak increases with higher temperature while the peaks at 33°, 47° and 56° decrease. The peak at 28° corresponds to the (111) plane in sphalerite ZnS and (112) in the kesterite structure. The peak with the same orientation ((222)/(224)) at 59° is overlapping with Mo but the intensity at this position also increases with

temperature. The Mo peak at  $74^\circ$ , which is free from overlap, shows that the signal from the Mo is fairly constant with temperature. This indicates that the intensity increase at  $59^\circ$  originates from the  $\Sigma$ -signal and that the film becomes more oriented towards the (111) or (112) plane with higher temperature. This kind of texture, with the closest packed plane horizontal to the substrate, is common for sputtered films [38]. The preferential orientation of the films also causes the XRD intensity to differ from the values given in the powder reference.

All the visible  $\Sigma$ -peaks are slightly shifted to lower angles while the peaks from the Mo-back contact are well aligned. The shift is largest for the room temperature deposition and decreases with higher temperature (Table III). At room temperature the shift is about 0.3 degrees compared to the kesterite reference. The shift in the peaks could have several origins. It was measured by XRF that the films change in composition with temperature and this could affect the size of the d-spacing. The sample with the most CZTS-like Cu/Sn-ratio is the sample where the peaks lie closest to the powder reference. However, the sample prepared with the heater set to  $300^\circ\text{C}$  is closest to CZTS in Zn- and sulfur content and this is further off from the reference. Sputtering quite commonly yields non-equilibrium phases and this could be another explanation for the peak shift. As discussed in [8] we suggest that the sputtered precursors could have a non-equilibrium phase with S-ions in the zinc-blende configuration and the metal ions randomly ordered at the cation sites. This would fit the XRD and Raman responses where a zinc-blende structure is observed with XRD but Raman suggests that each S atom is surrounded by 2:1:1 Cu:Zn:Sn, as in the kesterite structure. A random ordering of the cations would also mean a range of slightly different S environments causing a broadening of the Raman peak. Also in reference [8], Raman spectra were recorded using a 325nm (UV) excitation wavelength and this measurement strongly suggests the absence of the ZnS phase in the precursor. The enhanced surface diffusion at higher deposition temperatures makes it increasingly probable that the film will be in an equilibrium phase, more similar to the powder reference, and indeed we see that the shift is smallest for this deposition. However, the Raman looks similar for all depositions in this series. The XRD mismatch could also be due to compressive stress in the films. This would be consistent with the results from the bending of the thin glass substrates. The average of the stress measurement on the thin glass substrates (Table III) shows that all the films in the series are in compressive stress and that the stress is lowest for the high temperature deposition. However, as seen in Figure 7, the intermediate trend is different and the XRD peak shift shows a continuous decrease in stress while the curvature measurement indicates that only the highest temperature deposition has a significantly lower stress level. Due to possible errors in both methods it is hard to conclude anything else than the general trend and more work has to be done in order to exclude error sources.

These deposition series show the possibility to tune the precursor properties and give guidelines to which parameters to choose to get certain characteristics. Low stress and high density is usually preferable for thin films, which points towards the use of slightly elevated deposition temperatures. Limitations in the setup prevented us from investigating even higher temperature ranges in these experimental series. Another parameter, not studied in this paper, is additional ion bombardment of the growing film which is commonly used in other sputtering deposition processes. This could be used to further change the precursor properties.

#### 4. Conclusions

It was shown that it is possible to grow dense and homogeneous precursor films containing all elements for a CZTS-solar cell with reactive sputtering. Morphology, stress, metal and sulfur content were varied by changing the H<sub>2</sub>S/Ar-flow ratio, pressure and substrate temperature.

A process curve for the reactive sputtering of CZTS was presented and, as expected from sputtering theory, the discharge voltage and the deposition rate are strongly affected by the H<sub>2</sub>S/Ar- flow ratio. The Zn-target was shown to switch to compound mode earlier and more abruptly than the CuSn-target.

The films sputtered without H<sub>2</sub>S are crystalline and contain a CuZn-alloy and elemental Sn. Increasing the H<sub>2</sub>S/Ar-flow ratio gives amorphous films probably composed of a CuSn-alloy and ZnS. Further increasing the H<sub>2</sub>S partial pressure gives a columnar crystalline film, which shows zinc-blende peaks in XRD, a structure which is shared by ZnS, CTS and CZTS. The Raman scattering results best match CZTS.

Comparing different pressures and flows it was shown that the sulfur content is strongly dependent on the H<sub>2</sub>S partial pressure. The total pressures compared in this study have only a weak influence on the properties of the film. Differences can only be seen in the transition region between metal and compound mode where the system is very sensitive to changes.

Increasing the substrate temperature changes the film composition due to the high vapour pressures of Zn, SnS and S. High substrate temperatures also give slightly denser and increasingly oriented films. All the films in this series are under compressive stress but this is significantly lower for the highest substrate temperature (300 °C). Stress in the films could be important both for adhesion and grain growth and is therefore interesting for further studies.

#### Acknowledgements

The authors acknowledge financial support from the Swedish Energy Agency, Vinnova through the Vinnmer program and the Göran Gustafsson Foundation.

- [1] D.A. Barkhouse, O. Gunawan, T. Gokmen, T. Todorov, D. Mitzi, *Prog. Photovoltaics* 20/1 (2012) 6.
- [2] I. Repins, C. Beall, N. Vora, C. DeHart, D. Kuciauskas, P. Dippo, B. To, J. Mann, W.-C. Hsu, A. Goodrich, R. Noufi, *Sol. Energy Mater. Sol. Cells* 101/0 (2012) 154.
- [3] B. Shin, O. Gunawan, Y. Zhu, N.A. Bojarczuk, S.J. Chey, S. Guha, *Prog. Photovoltaics* 10.1002/pip.1174 (2011).
- [4] H. Katagiri, K. Jimbo, S. Yamada, T. Kamimura, W.S. Maw, T. Fukano, T. Ito, T. Motohiro, *Appl. Phys. Express* 1/4 (2008) 041201.
- [5] K. Wang, O. Gunawan, T. Todorov, B. Shin, S.J. Chey, N.A. Bojarczuk, D. Mitzi, S. Guha, *Appl. Phys. Lett* 97/14 (2010) 143508.
- [6] A. Ennaoui, M. Lux-Steiner, A. Weber, D. Abou-Ras, I. Kotschau, H.W. Schock, R. Schurr, A. Holzinger, S. Jost, R. Hock, T. Voss, J. Schulze, A. Kirbs, *Thin Solid Films* 517/7 (2009) 2511.
- [7] J.J. Scragg, T. Ericson, T. Kubart, M. Edoff, C. Platzer-Bjorkman, *Chem. Mater.* 23/20 (2011) 4625.

- [8] J.J. Scragg, T. Ericson, T. Kubart, M. Edoff, C. Platzer-Bjorkman, *Prog. Photovoltaics* (2012) To be published.
- [9] F.Y. Liu, K. Zhang, Y.Q. Lai, J. Li, Z.A. Zhang, Y.X. Liu, *Electrochem. Solid-State Lett.* 13/11 (2010) H379.
- [10] V. Chawla, B. Clemens, *IEEE Phot. Spec. Conf.* 35th (2010) 1902.
- [11] J.B. Li, V. Chawla, B.M. Clemens, *Adv. Mater.* 24/6 (2012) 720.
- [12] J.A. Thornton, D.G. Cornog, R.B. Hall, S.P. Shea, J.D. Meakin, *J. Vac. Sci. Technol., A* 2/2 (1984) 307.
- [13] J.A. Thornton, T.C. Lommasson, H. Talieh, B.H. Tseng, *Sol. Cells* 24/1-2 (1988) 1.
- [14] T. Watanabe, M. Matsui, *Jpn. J. Appl. Phys.* 35/3 (1996) 1681.
- [15] Y.B. He, T. Kramer, A. Polity, M. Hardt, B.K. Meyer, *Thin Solid Films* 431 (2003) 126.
- [16] Y.B. He, T. Kramer, I. Osterreicher, A. Polity, R. Gregor, W. Kriegseis, D. Hasselkamp, B.K. Meyer, *Jpn J Appl Phys* 2 41/4B (2002) L484.
- [17] S. Seeger, K. Ellmer, *Thin Solid Films* 517/10 (2009) 3143.
- [18] P.A. Flinn, D.S. Gardner, W.D. Nix, *IEEE Trans. Electron Devices* 34/3 (1987) 689.
- [19] S. Berg, T. Nyberg, *Thin Solid Films* 476/2 (2005) 215.
- [20] D. Depla, S. Heirwegh, S. Mahieu, J. Haemers, R. De Gryse, *J. Appl. Phys.* 101/1 (2007) 013301.
- [21] M. Ashraf, S. Ullah, S. Hussain, A.H. Dogar, A. Qayyum, *Appl. Surf. Sci.* 258/1 (2011) 176.
- [22] S. Seeger, K. Harbauer, K. Ellmer, *J. Appl. Phys.* 105/5 (2009) 053305.
- [23] J.A. Thornton, D.G. Cornog, R.B. Hall, L.C. Dinetta, *J. Vac. Sci. Technol.* 20/3 (1982) 296.
- [24] H.E. Swanson, E. Tatge, *Natl. Bur. Stand. (U.S.)* 539/1 (1953) 24.
- [25] J.K. Brandon, R.Y. Brizard, P.C. Chieh, R.K. Mcmillan, W.B. Pearson, *Acta Crystallogr., Sect. B: Struct. Sci.* B 30/Jun15 (1974) 1412.
- [26] C.Y. Chou, S.W. Chen, *Acta Mater.* 54/9 (2006) 2393.
- [27] E.A. Jumpertz, *Z Elektrochem* 59/5 (1955) 419.
- [28] M.H. Booth, J.K. Brandon, R.Y. Brizard, C. Chieh, W.B. Pearson, *Acta Crystallogr., Sect. B: Struct. Sci.* 33/Jan15 (1977) 30.
- [29] W.N. Schafer, R., *Mater. Res. Bull.* 9 (1974) 645.
- [30] L.S. Palatnik, I.F. Komnik, E.K. Belova, V.M. Koshkin, *Dokl. Akad. Nauk SSSR* 137/1 (1961) 68.
- [31] X.A. Chen, H. Wada, A. Sato, M. Mieno, *J. Solid State Chem.* 139/1 (1998) 144.
- [32] M. Onoda, X.A. Chen, A. Sato, H. Wada, *Mater. Res. Bull.* 35/9 (2000) 1563.
- [33] A. Weber, R. Mainz, H.W. Schock, *J. Appl. Phys.* 107/1 (2010) 013516.
- [34] H.E. Swanson, E. Tatge, *Natl. Bur. Stand. (U.S.)* 539/1 (1953) 20.
- [35] M. Himmrich, H. Haeuseler, *Spectrochim. Acta, Part A* 47/7 (1991) 933.
- [36] X. Fontane, L. Calvo-Barrio, V. Izquierdo-Roca, E. Saucedo, A. Perez-Rodriguez, J.R. Morante, D.M. Berg, P.J. Dale, S. Siebentritt, *Appl. Phys. Lett.* 98/18 (2011) 181905.
- [37] H.E. Swanson, E. Tatge, *Natl. Bur. Stand. (U.S.)* 539/I (1953) 16.
- [38] J.A. Thornton, *J. Vac. Sci. Technol.* 11/4 (1974) 666.
- [39] J.A. Thornton, D.W. Hoffman, *Thin Solid Films* 171/1 (1989) 5.

**Table I**

Process parameters, composition and thickness for series 1. The H<sub>2</sub>S/Ar-ratio was varied while power, process pressure and time were kept constant at 600 W for the CuSn-target, 330 W for the Zn-target, 0.67 Pa and 800 s respectively.

| Sample | H <sub>2</sub> S flow [sccm] | Ar flow [sccm] | Cu/Sn | Zn/(Cu+Sn) | S/Metals | Thickness [nm] |
|--------|------------------------------|----------------|-------|------------|----------|----------------|
| A      | 0                            | 20             | 1.90  | 0.49       | 0.03     | 960            |
| B      | 10                           | 10             | 1.86  | 0.16       | 0.44     | 1050           |
| C      | 15                           | 5              | 2.04  | 0.14       | 0.73     | 1170           |
| D      | 20                           | 0              | 1.99  | 0.21       | 1.03     | 830            |

**Table II**

Process parameters, composition and thickness for series 2. The influence of process pressure was investigated while power and time were kept constant at 600 W for the CuSn-target, 330 W for the Zn-target and 800 s respectively.

| Sample | H <sub>2</sub> S flow [sccm] | Ar flow [sccm] | Pressure [Pa] | Cu/Sn | Zn/(Cu+Sn) | S/Metals | Thickness [nm] |
|--------|------------------------------|----------------|---------------|-------|------------|----------|----------------|
| E-5    | 10                           | 20             | 0.67          | 2.09  | 0.28       | 0.30     | 1140           |
| E-10   | 10                           | 20             | 1.33          | 1.87  | 0.32       | 0.35     | 1030           |
| F-5    | 20                           | 10             | 0.67          | 2.02  | 0.15       | 0.82     | 1310           |
| F-10   | 20                           | 10             | 1.33          | 1.94  | 0.14       | 0.96     | 1620           |
| G-5    | 30                           | 0              | 0.67          | 2.02  | 0.24       | 1.17     | 760            |
| G-10   | 30                           | 0              | 1.33          | 1.99  | 0.28       | 1.22     | 800            |

**Table III**

Process parameters and film characteristics for series 3. The substrate temperature was varied while power, process pressure, gas flow and time were kept constant at, 520 W for the CuSn-target, 480 W for the Zn-target, 0.67 Pa, 20 sccm H<sub>2</sub>S (no Ar) and 1800 s, respectively. The stress values were calculated from the curvature measurement and are an average of both measurement directions. The XRD peak values show the shift away from the ZnS/CZTS powder reference, which decreases with rising substrate temperature. The density was calculated from the metal atom amount from XRF using the RBS calibration, the EDS measurement of sulfur content and the thickness measured with the Dektak/SEM cross sections.

| Heater temp [°C] | Estimated substrate temp [°C] | Cu/Sn | Zn/(Cu+Sn) | S/ Metals | Thickness [nm] | Avg. stress [MPa] | Peak position XRD [°] | Density [g/cm <sup>3</sup> ] |
|------------------|-------------------------------|-------|------------|-----------|----------------|-------------------|-----------------------|------------------------------|
| 40               | 30                            | 1.60  | 0.39       | 1.09      | 1030           | -429              | 28.22                 | 4.12                         |
| 100              | 60                            | 1.61  | 0.38       | 1.10      | 1030           | -457              | 28.27                 | 4.08                         |
| 200              | 120                           | 1.64  | 0.37       | 1.08      | 890            | -424              | 28.28                 | 4.37                         |
| 300              | 180                           | 1.73  | 0.33       | 1.01      | 870            | -488              | 28.30                 | 4.48                         |
| 400              | 240                           | 1.86  | 0.29       | 0.998     | 850            | -388              | 28.29                 | 4.54                         |
| 500              | 300                           | 1.91  | 0.26       | 0.928     | 750            | -195              | 28.35                 | 4.55                         |

## Figures

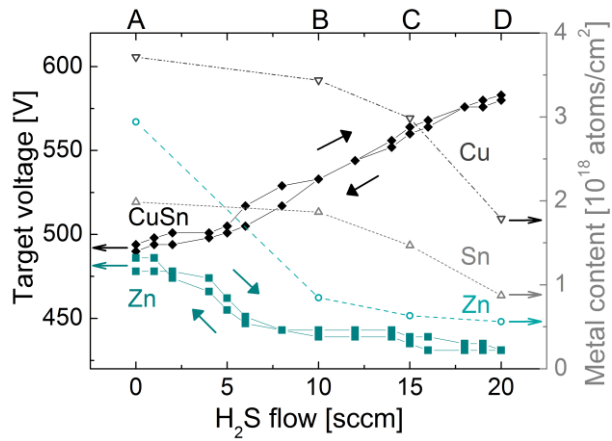


**Figure 1**

Process curve for co-sputtering CuSn and Zn in a pressure of 0.67 Pa and a total flow of 20 sccm (the H<sub>2</sub>S flow shown on the x-axis was complemented with Ar-flow to a constant sum of 20 sccm). These were also the conditions used in Series 1 where samples were made at the H<sub>2</sub>S flows indicated by the letters at the top (all other parameters were kept constant). The dotted/dashed lines and the right axis show the metal content of the samples, measured by XRF and converted to areal density by the RBS calibration.

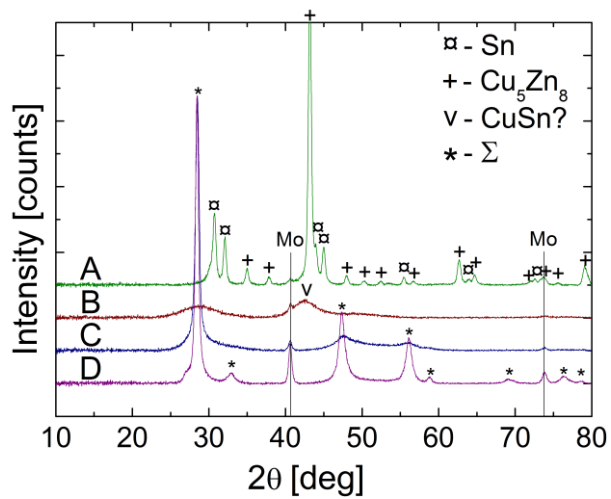


**Figure 2**

Grazing incidence XRD on Series 1. Sample A was sputtered without  $\text{H}_2\text{S}$  and shows reflections from  $\text{Cu}_5\text{Zn}_8$  and Sn. The B sample is mostly amorphous but the broad peaks fit the most intense peaks of ZnS and CuSn. The two most sulfur rich precursors show peaks common between ZnS, CTS and CZTS, called  $\Sigma$  signal.

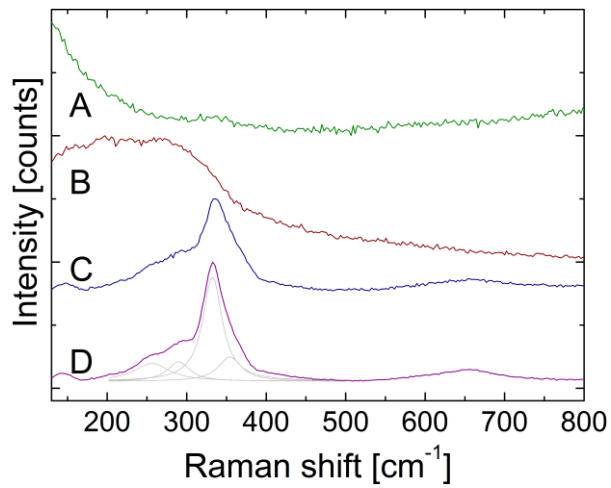


**Figure 3**

Raman scattering from Series 1. The two samples with highest sulfur content, C and D, show a broad peak at 336 and 332 and  $\text{cm}^{-1}$  respectively. For sample D peak fitting with Lorentzian curves shows four peaks between 200 and 500  $\text{cm}^{-1}$ . The resulting peak positions for the weaker contributions are at 256  $\text{cm}^{-1}$ , 290  $\text{cm}^{-1}$  and 354  $\text{cm}^{-1}$ .

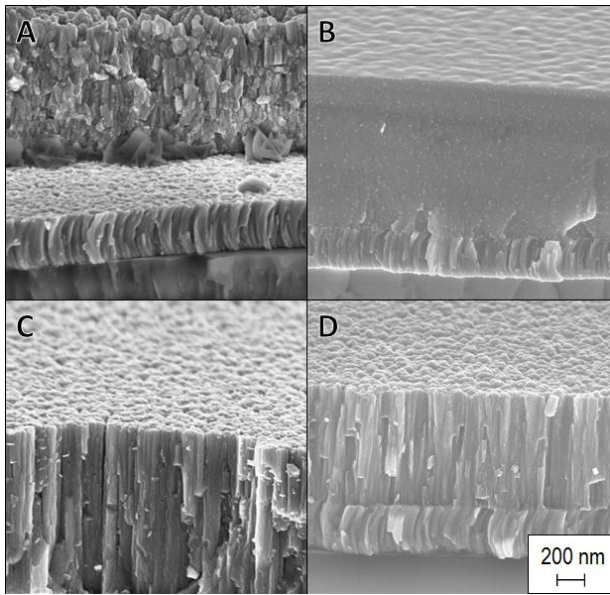


**Figure 4**

SEM cross sections on Series 1 with increasing fraction of  $\text{H}_2\text{S}$  in the sputtering atmosphere.

The morphology changes from disordered crystalline through amorphous to columnar crystalline. The layer underneath the film is the Mo back contact.

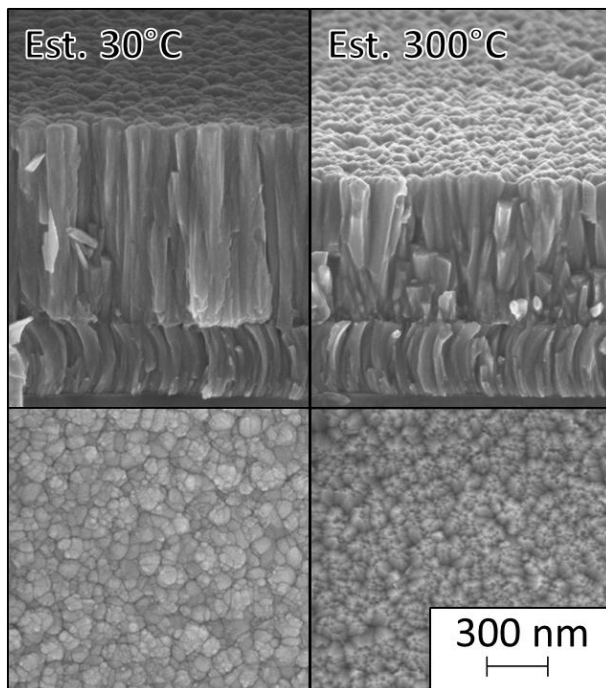


**Figure 5**

SEM images of the room temperature (to the left, cross section and top view) and the highest temperature (to the right, cross section and top view) sample in Series 3. It can be seen that the high temperature sample is thinner and has a more faceted surface. The layer underneath is the Mo back contact.

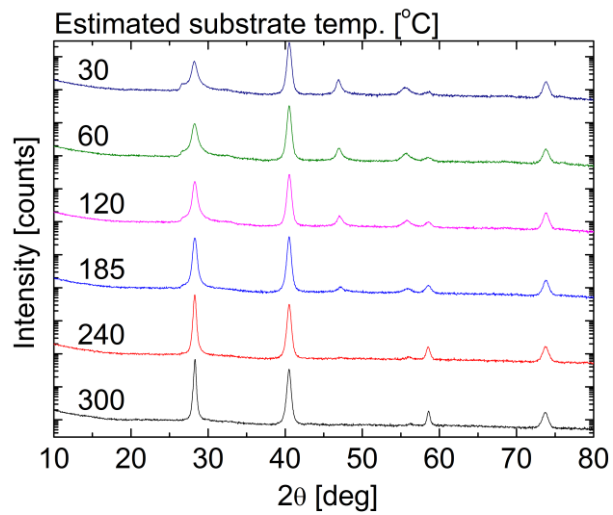


**Figure 6**

XRD from Series 3. Higher temperature yields a more oriented film. The Mo-peaks agrees well with the powder reference while the peaks from ZnS/CZTS are slightly shifted to lower angles. See also Table III.

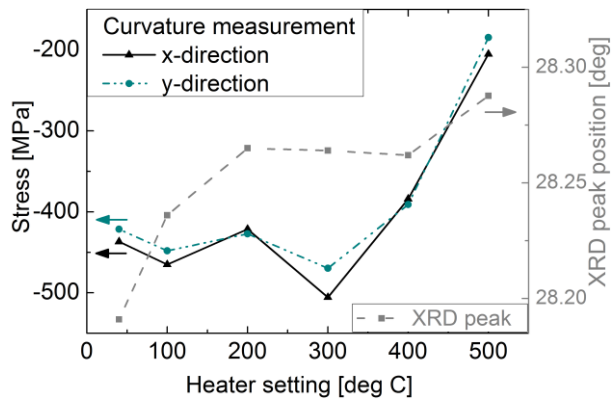


**Figure 7**

Stress values measured by evaluating the curvature of a thin glass substrate before and after deposition. The curvature was measured in two perpendicular directions. XRD was measured on samples on rigid glass from the same deposition runs.